

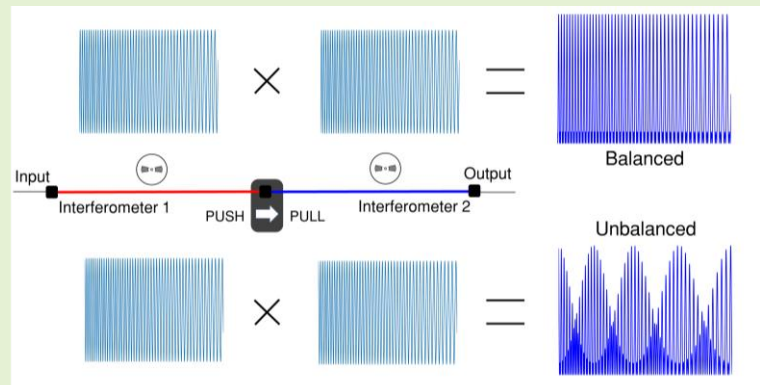
# Colossal enhancement of strain sensitivity using the push-pull deformation method

Paulo Robalinho, André Gomes, and Orlando Frazão

**Abstract**— In this work, a colossal enhancement of strain sensitivities through the push-pull deformation method in interferometry is reported for the first time. For the demonstration of the new method, two cascaded interferometers in a fiber loop mirror are used. Usually, strain is applied at the fiber end of the interferometers. In this work, we propose applying strain at the middle of the two cascaded interferometers whereas the fiber ends of the sensor are fixed. Strain is then applied in the fusion region between the two-cascaded interferometers in a push-pull configuration, thus ensuring simultaneously the extension of one interferometer and the compression of the other.

Although the carrier signal is maintained constant, the proposed technique induces a colossal enhancement of sensitivity in the envelope signal. Strain sensitivities up to  $10000 \text{ pm}/\mu\epsilon$  are achieved.

**Index Terms**— fiber loop mirror, optical fiber sensor, strain optical sensor, Vernier effect



## I. Introduction

THE technological development allowed the precise quantification of physical, chemical, and biological parameters. Despite several technological advances throughout history, the appearance of new optical technologies [1,2] began to have a high impact in the society. The emergence of optical fibers performed an important role in optical communications, biomedical, and harsh environment applications [3,4]. With the improvement of manufacturing techniques and development of new materials, new orders of sensitivity have been possible to achieve. The term giant, present in scientific literature, is used to express an improvement by a factor equal to or higher than 5 times. However, there are also articles that apply the term giant with factors less than 5 times, but the increment obtained is higher than the average increment obtained in the scientific area. Examples of giant sensitivities in optical sensor (considerably improved over previous cases) are sensors that involve mode loss [5], mode transfer near the turning point of a long period grating (LPG) [6], and giant resonances in optical

microstructures [7], as well as the appearance of giant optical nonlinearities [8]. These recent advances represent new solutions for medicine [9] and biology [10]. Interferometry has an important role for sensing and, combined with novel configurations [11,12], the properties of interferometers can be easily controlled. The cascade design is the most popular, with applications in lasers [13], sensors [14], and filters [15].

Recently, the first optical fiber interferometric sensors based on beat measurements called Vernier effect [17] and Harmonic Vernier effect [18] were published. This phenomenon relies on the overlap between different signals [19]. In interferometry, the overlap between the fringes of different interferometers gives rise to two new waves: the envelope and the carrier. From a sensing perspective the envelope has typically a magnified sensitivity. A big issue in interferometry is the balancing of the optical system. One solution is the push-pull technique [20] where, to obtain a balance, one of the optical paths is expanded or compressed in order to optimize the system. This technique is present, not only in communication systems with the purpose of frequency synchronization [21] and optical signals modulation [22], but also in accelerometer [23], hydrophones [24], acoustic and vibration sensors [25] in optical fibers. Another denomination for push-pull is the compression and expansion in hysteresis cycles [26], or the conversion of compression into expansion used in microdevices [27].

Recently, strain sensors in optical fiber reporting high sensitivities using the optical Vernier effect were demonstrated. Examples of such structures are a hollow microsphere coupled to a capillary, originating two FPIs, with

Manuscript received XXX XX, XXXX; accepted XXX XX, XXXX. Date of publication XXX XX, XXXX; date of current version XXX XX, XXXX. This work is financed by National Funds through the Portuguese funding agency, FCT - Fundação para a Ciência e a Tecnologia, within project UIDB/50014/2020. André Gomes is funded by FCT (SFRH/BD/129428/2017).

The authors are with the is with INESC TEC and Department of Physics and Astronomy, Faculty of Sciences, University of Porto, Rua do Campo Alegre 687, 4169-007 Porto, Portugal (e-mail: [ofraza@inesctec.pt](mailto:ofraza@inesctec.pt)).

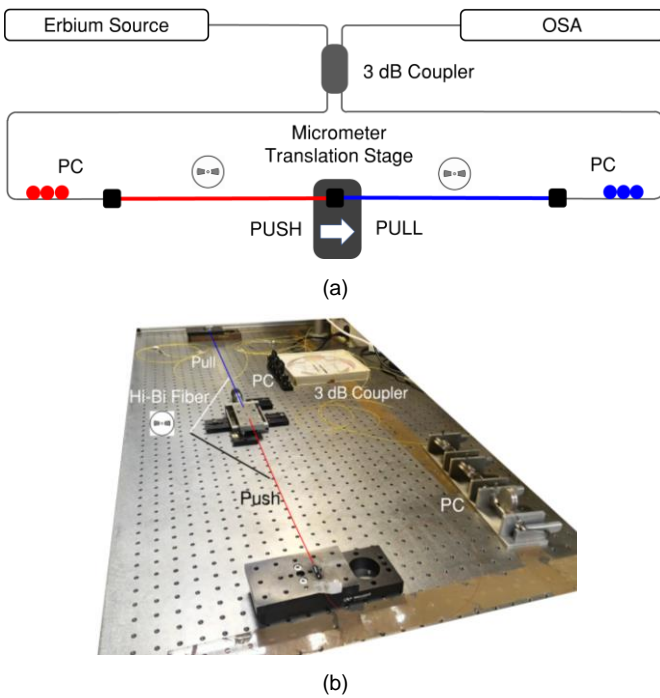


Fig. 1. Experimental setup configuration with two cascaded interferometers inside a fiber loop mirror: (a) scheme and (b) picture. The deformation is applied using a translation stage placed between the two interferometers.

a sensitivity of  $146.3 \text{ pm}/\mu\epsilon$  for a range of  $600 \mu\epsilon$  [28] and 2-fiber loop mirrors in series with a sensitivity of  $120 \text{ pm}/\mu\epsilon$  for a range of  $1000 \mu\epsilon$  [29].

In this work, a push-pull deformation method applied to two cascaded interferometers is presented. As demonstration, two cascaded non-balanced Mach-Zehnder interferometers in a fiber loop configuration are used. Currently, the deformation is typically applied at the sensor ends. Our new proposal is disruptive as the deformation is applied in the middle of the sensing head. Thereby, a push-pull configuration is obtained when the deformation is applied at the splice region between the two cascaded interferometers. This configuration guarantees simultaneously the expansion and compression of the two interferometers. Under these conditions an enhanced Vernier effect [30], that induces a colossal enhancement of strain sensitivity of the generated envelope modulation, is introduced leading to a 68-fold increase of sensitivity compared to current sensors.

## II. SENSOR SETUP AND THEORETICAL MODEL

To validate this method that combines the Vernier effect and the push-pull deformation method, we adopted a configuration based on a fiber loop mirror. In Fig. 1, we show the experimental setup configuration used for the demonstration. A broadband erbium source is used to illuminate the interferometers.

Two cascaded non-balanced Mach-Zehnder interferometers in a fiber loop configuration are formed by a 3 dB fiber coupler and two sections of high-birefringent (Hi-Bi) fibers. Both Hi-Bi fibers that form the two interferometers are bow-tie fiber sections with a length of  $(1.251 \pm 0.001) \text{ m}$  with a

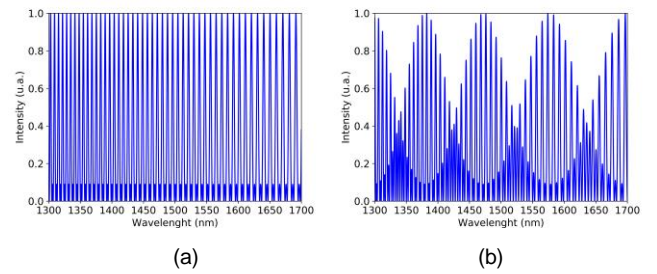


Fig. 2. Simulation considering a  $L_{\text{fiber}} = 1.252 \text{ m}$  and  $\beta = 4.35 \times 10^{-4}$ : (a) balanced system and (b) unbalanced system.

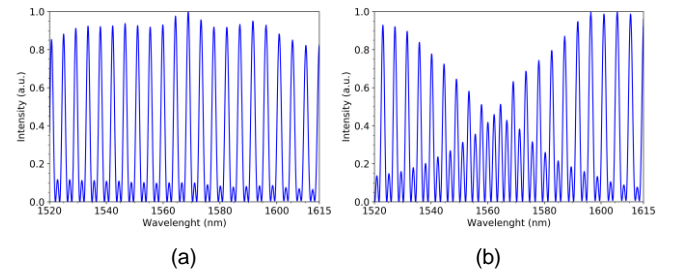


Fig. 3. Experimental results for two situations: (a) balanced system and (b) unbalanced system.

birefringence of  $\beta = 4.35 \times 10^{-4}$ . Since Hi-Bi fibers are sensitive to the polarization state of the propagating light, two polarization controllers were used in order to maximize the visibility of the output beam. To ensure that we have two independent interferometers, the two Hi-Bi fibers must be spliced together with the polarization axes of one Hi-Bi fiber rotated by  $\pi/2$  in relation to the polarization axes of the other Hi-Bi fiber. The push-pull deformation method consists in applying deformation between the two-cascaded interferometers when both are initially pre-stretched. In Fig. 1, we also indicate the position of the micrometric translation stage, which is located between the two sections of Hi-Bi fiber. The translation stage is used to apply strain to the structure, through manual action. When a push-pull deformation is applied, one of the interferometers is extended and the other is simultaneously compressed. The push-pull deformation method can be used in both ways and a large deformation range up to around  $2.5 \text{ m}\epsilon$ .

Considering the features of the system, the theoretical model is described by:

$$\frac{E_{\text{out}}}{E_{\text{in}}} \propto A(e^{-i\beta_{x_1}L_1} + e^{-i\beta_{y_1}L_1})(e^{-i\beta_{x_2}L_2} + e^{-i\beta_{y_2}L_2}) - B e^{-i\pi/2} (e^{-i\beta_{x_2}L_2} - e^{-i\beta_{y_2}L_2})(e^{-i\beta_{x_1}L_1} - e^{-i\beta_{y_1}L_1}) e^{-i\pi/2} \quad (1)$$

where  $\beta_{xi} = 2\pi n_{xi}/\lambda$  and  $\beta_{yi} = 2\pi n_{yi}/\lambda$ . Thus,

$$\frac{I_{\text{out}}}{I_{\text{in}}} \propto \left\{ A \left[ \cos\left(\frac{\pi}{\lambda}\beta L_1\right) \cos\left(\frac{\pi}{\lambda}\beta L_2\right) \right] - B \left[ \sin\left(\frac{\pi}{\lambda}\beta L_1\right) \sin\left(\frac{\pi}{\lambda}\beta L_2\right) \right] \right\}^2 \quad (2)$$

where  $\beta_i = n_{yi} - n_{xi}$ . For this system,  $A = 1$  and  $B = 0.15$  and result

$$\frac{I_{\text{out}}}{I_{\text{in}}} \propto \left[ 1.15 \cdot \cos\left(\frac{\pi}{\lambda}\beta[L_1 + L_2]\right) + 0.85 \cdot \cos\left(\frac{\pi}{\lambda}\beta[L_1 - L_2]\right) \right]^2 \quad (3)$$

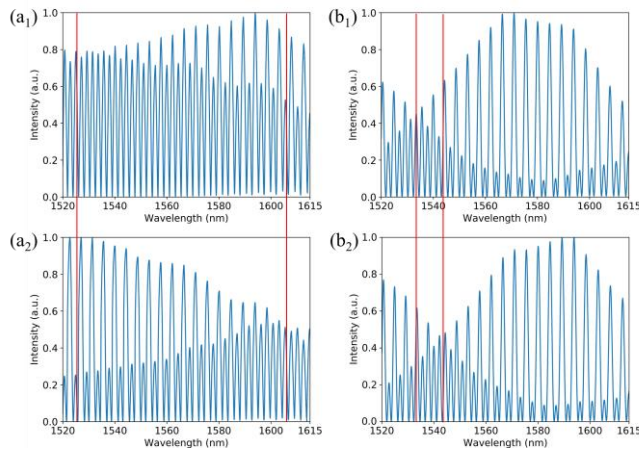


Fig. 4. (a) Output spectra for  $\beta L_1 \approx \beta L_2$ . (b) Output spectra for  $\beta L_1 \neq \beta L_2$ ; Index 1 and 2 refer to two consecutive steps, when a push-pull deformation of  $8 \mu\epsilon$  is applied (corresponding to a translation stage displacement of  $10 \mu\text{m}$ ).

Fig. 2 (a) presents the spectral results obtained by the equation 3 where the interferometer is balanced or (b) unbalanced.

The spectral shift of the envelope with a carrier signal constant shift can be explained by the mathematical expressions that influences these two components in equation 3. The carrier signal is proportional to  $\cos[\pi/\lambda \cdot \beta(L_1+L_2)]$ , while the envelope modulation is decided by  $\cos[\pi/\lambda \cdot \beta(L_1-L_2)]$ . The push-pull deformation method corresponds to the compression of one interferometer, while the other is extended, resulting in the enhanced Vernier effect implementation [30]. On one hand, the sum of the variation of both lengths is null ( $\Delta L_1 + \Delta L_2 = 0$ ), resulting in a constant carrier signal. On the other hand, the difference between the variation of both lengths adds up ( $\Delta L_1 - \Delta L_2 \neq 0$ ), considering that the two interferometers have opposite deformation response, resulting in a large envelope modulation shift.

### III. EXPERIMENTAL RESULTS

Fig. 3 presents the experimental results of these two situations. The spectral response of the balanced cascaded interferometers, i.e. the optical path of both interferometers is the same ( $\beta L_1 = \beta L_2$ ), is shown in Fig. 3(a). This balanced condition, where the cascaded interferometers are pre-stretched and their lengths are approximately the same, is considered the “zero” strain. When deformation is applied to the cascaded interferometers using the push-pull method, the initial condition changes, and the optical path of the two interferometers is then different ( $\beta L_1 \neq \beta L_2$ ). In this case, the spectral response of the cascaded interferometers is unbalanced and generates an envelope modulation due to the Vernier effect in the output spectrum, as shown in Fig. 3(b). The response of the envelope modulation as a function of the applied strain to both directions using the push-pull deformation method was studied.

For a better explanation of this effect, two different spectra of the non-balanced cascaded interferometers in distinct sensitivity regions are presented in Fig. 4. Fig. 4(a<sub>1</sub>) is a spectrum when the system is close to the balanced situation, and applying a push-pull deformation of  $8 \mu\epsilon$ , corresponding to a  $10 \mu\text{m}$  displacement of the translation stage (minimum

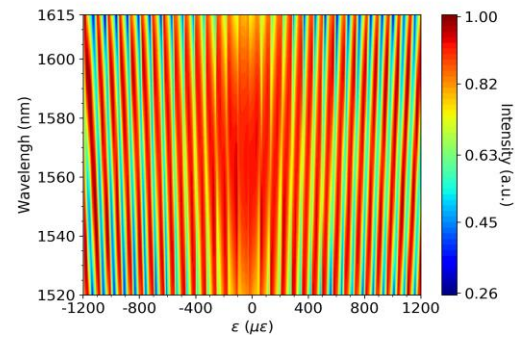


Fig. 5. 2D plot of the envelope modulation as a function of the applied strain. The envelope presents a colossal sensitivity (given by the slope of the red lines) near the  $0 \mu\epsilon$  region.

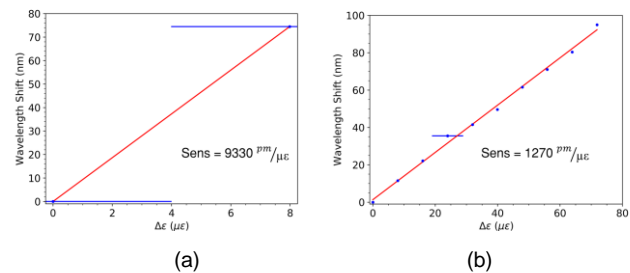


Fig. 6. Strain response of the interferometry. a) Colossal sensitivity and b) high sensitivity.

displacement allowed by the translation stage), the resultant output spectra represent in Fig. 4(a<sub>2</sub>). The same for Fig. 4(b<sub>1</sub> and b<sub>2</sub>), but in this case the system is further away from the balanced situation (i.e. unbalanced). Comparing all the spectra in Fig. 4(a) and 4(b), we can observe that, the larger the envelope modulation is, the closer we are to the colossal sensitivity region, and therefore the longer is the wavelength shift of the envelope.

In Fig. 5, a 2D plot exhibiting the position of the envelope with the applied deformation is presented. The strain sensitivity of the envelope can be obtained, for example, by taking the slope of the minimum envelope intensity as a function of the applied strain. A colossal strain sensitivity region can be obtained when the optical paths of the cascaded interferometers are very close, i.e. near the initial situation where the two interferometers are balanced (around  $0 \mu\epsilon$ ). The further we move away from this region, by applying deformation, the smaller the sensitivity becomes (smaller slope).

All the following linear adjustments have a  $r^2$  higher than 0.99. The sensitivity values are very different for each case. For the first case, represented in Fig. 6(a), we achieved a colossal strain sensitivity of  $9330 \text{ pm}/\mu\epsilon$ , since the situation is close to the case where the interferometers are balanced. As for Fig. 6(b), we obtained strain sensitivities of  $1270 \text{ pm}/\mu\epsilon$ , corresponding this last case to a situation further away from the colossal sensitivity region. Important is to mention that, for each situation the range of applied strain is different. In the giant sensitivity region, the range of applied strain is limited a  $10 \mu\epsilon$ , while for the other regions the range can be increase up

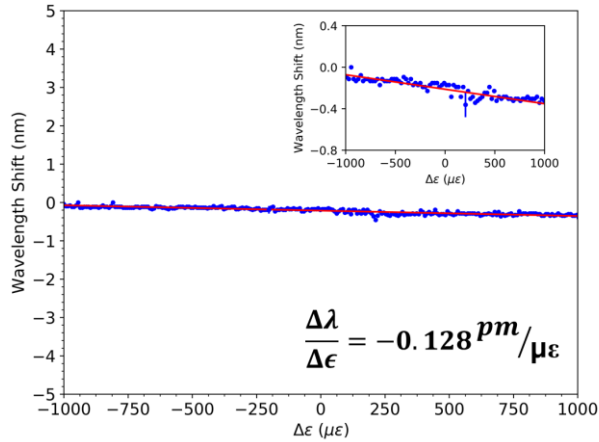


Fig. 7. Wavelength shift of the carrier signal as a function of applied deformation. A strain sensitivity of  $pm/\mu\epsilon$  along the whole range of applied strain studied is obtained.

to  $1000 \mu\epsilon$ . During all the experiments we observe that the carrier signal was approximately constant, as we report in Fig. 7. The strain sensitivity of the carrier is  $(-0.128 \pm 0.004) pm/\mu\epsilon$  in all the applied strain range studied. This result is expectable due to the carrier sensitivity being dependent on the sum of sensitivity of each interferometer. Although the fibers have the same sensitivity, as this new method allows to have opposite mechanical actions, that is, while one fiber is pulled the other is pushed, then allows to obtain symmetric sensitivities. Thus, the carrier sensitivity is zero.

Comparing the strain sensitivity of the carrier signal with the traditional configuration using a single Hi-Bi fiber in a fiber loop mirror, with a linear strain sensitivity of  $(29.31 \pm 0.01) pm/\mu\epsilon$ , the sensitivity of the carrier signal can be negligible. In Fig. 8, we represent the strain sensitivity across the whole strain range studied. The strain sensitivity of the envelope modulation changes with the push-pull deformation method, from a low value of  $(1160 \pm 30) pm/\mu\epsilon$  to a maximum value of  $(10100 \pm 100) pm/\mu\epsilon$ . The red line represents the theoretical behavior expected. Comparing with conventional configuration Vernier effect [31] where the envelope presents  $59 pm/\mu\epsilon$ , this push-pull deformation method increase is more than 170 times higher. This behavior is similar for temperature response [32].

An important factor that allows to compare the sensitivity of the envelope with the sensitivity of each sensor is the  $M$ -factor, given by  $M = Sens_{env} / Sens_1$  [18]. For this system,  $M$ -factor is 341. However, if we are not in the traditional Vernier effect, this factor alone does not allow a correct evaluation of the Vernier effect implementation. So, two new factors arise [29], namely:  $M_{FSR} = \Delta\lambda_{env} / \Delta\lambda_{car}$  and  $M_{sens} = sens_{env}/sens_{carr}$ . Thus:

$$M_{Vernier} = M_{Sens}/M_{FSR} \quad (4)$$

The carrier  $FSR$  is  $2.5 nm$  and the minimum envelope  $FSR$  is  $90 nm$ , resulting in an  $M_{FSR}$ -factor of 36. Considering the sensitivity presented in Fig. 7, the minimum  $M_{Sens}$ -factor is 9062 (worst case scenario presented, corresponding to an envelope sensitivity of  $1160 pm/\mu\epsilon$ ), which implies that

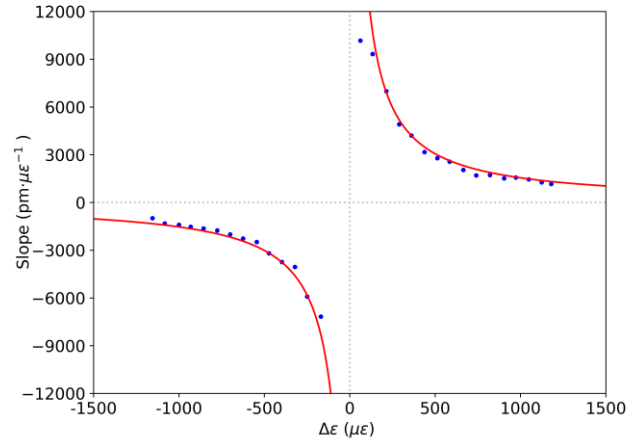


Fig. 8. Strain sensitivity of the envelope modulation along the whole range of applied deformation studied. The sensitivity changes with the applied deformation, being colossal in a short region close to the initial balanced case of  $0 \mu\epsilon$ . All sensitivities are obtained based on linear adjustments with  $r^2$  higher than 0.99.

$M_{Vernier}$  is 251 ( $\gg 1$ ). Therefore, the proposed method achieves a Vernier effect much more efficient than the traditional Vernier effect methods used.

Another important factor is the stability of the results. It is clear that, given their colossal sensitivity, parasitic nanometric vibrations will influence the measurements accuracy. In addition, another important factor is temperature. In this case, the sensitivity to temperature is the same in both fibers (unlike to the strain sensitivity which are symmetrical due to the push-pull method). Based on the end of Section II, if the sensitivities of the two fibers are equal, the impact on the measurements will not be on the envelope but on the carrier. Therefore, since this work focuses on the measurement of the envelope wave, the impact of temperature is approximately null. Through Fig. 7, the carrier wave variation was  $-0.36 nm$  and linear during the experimental work. Considering that the temperature sensitivity of Hi-Bi fiber is  $-1.23 nm/^\circ C$  [32] and recalling that the carrier has double the temperature sensitivity compared with a single Hi-Bi fiber, then the fibers were subjected to a temperature variation of only  $0.15 ^\circ C$ .

#### IV. CONCLUSIONS

In sum, a push-pull deformation method allows high performance to be achieved by means of enhanced Vernier effect. As a result, sensitivities of  $10000 pm/\mu\epsilon$  are obtained corresponding to an  $M$ -factor of 341 and  $M_{Vernier}$ -factor of 251, being this last valor a record. In addition, this sensor is 68-fold more sensitive than current optical fiber strain sensors. This new method is easily demonstrated using large Hi-Bi fiber length in a Fiber Loop Mirror configuration. Since the minimum resolution of OSA is  $0.02 nm$ , then the minimum resolution of this two-cascaded interferometer is  $2 n\epsilon$ . This new push-pull deformation method allows to study the limits of the Vernier effect in order to obtain colossal sensitivities, opening new opportunities for the development of new architectures of strain sensors, accelerometers, gyroscopes, microphones, hydrophones for applications from biology to

engineering, in addition to gravity measurements. Finally, this method can be use in any configuration in interferometry since a beat signal can be create when the two interferometers are non-balanced.

## REFERENCES

- [1] S. D. Smith, "Lasers, nonlinear optics and optical computers", *Nature*, vol. 316, pp. 319-324, July 1985, DOI: 10.1038/316319a0.
- [2] C. P. Christensen, "New Laser Source Technology", *Science*, vol. 224, no. 4645, pp. 117-123, Apr. 1984, DOI: 10.1126/science.224.4645.117.
- [3] J. I. Peterson, G. G. Vurek, "Fiber-optic sensors for biomedical applications", *Science*, vol. 224, no. 4645, pp. 123-127, Apr. 1984, DOI: 10.1126/science.6422554.
- [4] R. Pirich, K. D'Ambrosio, May 2011, "Fiber optics for harsh environments", IEEE Long Island Systems, Applications and Technology Conference, DOI: 10.1109/LISAT.2011.5784241.
- [5] F. J. Arregui, I. D. Villar, C. R. Zamarreño, P. Zubiate, I. R. Matias, "Giant Sensitivity of Optical Fiber Sensors by means of Lossy Mode Resonance", *Sensors and Actuators B: Chemical*, vol. 232, pp. 660-665 Sept. 2016, DOI: 10.1016/j.snb.2016.04.015.
- [6] P. Pilla, C. Trono, F. Baldini, F. Chiavaioli, M. Giordano, A. Cusano, "Giant sensitivity of long period gratings in transition mode near the dispersion turning point: an integrated design approach", *Optics Letters* vol. 37, iss. 19, pp. 4152-4154, Oct. 2012, DOI: 10.1364/OL.37.004152.
- [7] Y. Li, O. V. Svitelskiy, A. V Maslov, D. Carnegie, E. Rafailov, V. N. Astratov, "Giant resonant light forces in microspherical photonics", *Light Sci. Appl.*, vol. 2, no. e64, Apr. 2013, DOI: 10.1038/lsa.2013.20.
- [8] S. Houverl, A. Lebreton, T. A. S. Pereira, G. Xu, R. Colombelli, I. Kundu, L. H. Li, E. H. Linfield, A. G. Davies, J. Mangeney, J. Tignon, R. Ferreira, S. S. Dhillon, "Giant optical nonlinearity interferences in quantum structures", *Science Advances*, vol. 5, no. 10, eaaw7554, Oct. 2019, DOI: 10.1126/sciadv.aaw7554.
- [9] D. Murzin, D. J. Mapps, K. Levada, V. Belyaev, A. Omelyanchik, L. Panina, V. Rodionova, "Ultrasensitive Magnetic Field Sensors for Biomedical", *Sensors*, vol. 20, iss. 6, no. 1569, Mar. 2020, DOI: 10.3390/s20061569.
- [10] D. K. Wood, K. K. Ni, D. R. Schmidt, A. N. Cleland, "Submicron giant magnetoresistive sensors for biological applications", *Sensors and Actuators A: Physical*, vol. 120, iss. 1, pp. 1-6, Apr. 2005, DOI: 10.1016/j.sna.2004.10.035.
- [11] C. Trono, F. Baldini, M. Brenci, F. Chiavaioli, M Mugnaini, "Flow cell for strain- and temperature-compensated refractive index measurements by means of cascaded optical fibre long period and Bragg gratings", *Meas. Sci. Technol.*, vol. 22, no. 075204, June 2011, DOI: 10.1088/0957-0233/22/7/075204.
- [12] T. Nan, Bo Liu, Y. Wu, J. Wang, Y. Mao, L. Zhao, T. Sun, J. Wang, "Ultrasensitive strain sensor based on Vernier- effect improved parallel structured fiber-optic Fabry-Perot interferometer", *Optics Express*, vol. 27, iss. 12, pp. 17239-17250, June 2019, DOI: 10.1364/OE.27.017239.
- [13] M. Seidel, X. Xiao, S. A. Hussain, G. Arisholm, A. Hartung, K. T. Zawilski, P. G. Schunemann, F. Habel, M. Trubetskov, V. Pervak, O. Pronin, F. Krausz, "Multi-watt, multi-octave, mid-infrared femtosecond source", *Science Advances*, vol. 4, no. 4, Apr. 2018, DOI: 10.1126/sciadv.aaq1526.
- [14] W. Zhang, W. Zhuang, M. Dong, L. Zhu, F. Meng, "Dual-Parameter Optical Fiber Sensor for Temperature and Pressure Discrimination Featuring Cascaded Tapered-FBG and Ball-EFPI", *IEEE Sensors Journal*, vol. 19, iss. 14, pp. 5645-5652, July 2019, DOI: 10.1109/JSEN.2019.2905635.
- [15] V. R. Supradeepa, C. M. Long, R. Wu, F. Ferdous, E. Hamidi, D. E. Leaird, A. M. Weiner, "Comb-based radiofrequency photonic filters with rapid tunability and high selectivity", *Nature Photon*, vol. 6, pp. 186-194, Mar 2012, DOI: 10.1038/nphoton.2011.350.
- [16] W. Xu, J. Wang, J. Zhao, C. Zhang, J. Shi, X. Yang, J. Yao, "Reflective Liquid Level Sensor Based on Parallel Connection of Cascaded FBG and SNCS Structure", *IEEE Sensors Journal*, vol. 17, iss. 5, pp. 1347-1352, Nov. 2017, DOI: 10.1109/JSEN.2016.2629488.
- [17] X. Zhang, L. Ren, X. Wu, H. Li, L. Liu, L. Xu, "Coupled optofluidic ring laser for ultrahigh- sensitive sensing", *Optics Express*, vol. 19, iss. 22, pp. 22242-22247, Oct 2011, DOI: 10.1364/OE.19.022242.
- [18] A. D. Gomes, M. S. Ferreira, J. Bierlich, J. Kobelke, M. Rothhardt, H. Bartel, O. Frazão, "Optical Harmonic Vernier Effect: A New Tool for High Performance Interferometric Fiber Sensors", *Sensor*, vol. 19, iss. 24, no. 5431, Dec 2019, DOI: 10.3390/s19245431.
- [19] M. La Notte, V. M. N. Passaro, "Ultra high sensitivity chemical photonic sensing by Mach-Zehnder interferometer enhanced Vernier-effect", *Sensors and Actuators B: Chemical*, vol. 176, pp. 994-1007, Jan. 2013, DOI: 10.1016/j.snb.2012.10.008.
- [20] R. Briguglio, F. Q.-Pacheco, J. R. Males, M. Xompero, A. Riccardi, L. M. Close, K. M. Morzinski, S. Esposito, E. Pinna, A. Puglisi, L. Schatz, K. Miller, "Optical calibration and performance of the adaptive secondary mirror at the Magellan telescope", *Sci Rep*, vol. 8, no. 10835, July 2018, DOI: 10.1038/s41598-018-29171-6.
- [21] R. Slavik, S. G. Farwell, M. J. Wale, D. J. Richardson, "Compact Optical Comb Generator Using InP Tunable Laser and Push-Pull Modulator", *IEEE Photonics Technology Letters*, vol. 27, iss.2, pp. 217-202, Jan 2014, DOI: 10.1109/LPT.2014.2365259.
- [22] G. de Valicourt, C.-M. Chang, J. Lee, M. S. Eggleston, C. Zhu, J. H. Sinsky, K. Kim, Po Dong, A. Maho, R. Brenot, Y.-K. Chen, "Integrated Hybrid Wavelength-Tunable III-V/Silicon Transmitter Based on a Ring-Assisted Mach-Zehnder Interferometer Modulator", *Journal of Lightwave Technology*, vol. 36, iss. 2, pp. 204-209, Jan. 2017, DOI: 10.1109/JLT.2017.2787763.
- [23] Yi Duo, He Xiangge, L. Fei, Gu Lijuan, Z. Min, Q. Xiaokang, Ye Han, "Self-suppression of common-mode noises of the different fiber optic interferometric accelerometers", *Optics Express*, vol. 26, iss. 12, pp. 15384-15397, Jun 2018, DOI: 10.1364/OE.26.015384.
- [24] S. Niu, Y. Hu, Z. Hu, H. Luo, "Fiber Fabry-Pérot Hydrophone Based on Push-Pull Structure and Differential Detection", *IEEE Photonics Technology Letters*, vol. 23, iss. 20, pp. 1499-1501, Oct. 2011, DOI: 10.1109/LPT.2011.2162645.
- [25] P. V. Skliarov, A. A. Davidenko, Y. A. Ogryzko, L. B. Liokumovich, Oct. 2019, "Phase Difference Measurement of the Target Signals of Sensing Elements in the Push-Pull Fiber Optic Interferometric Acoustic and Vibration Sensors", IEEE International Conference on Electrical Engineering and Photonics (EExPolytech), DOI: 10.1109/EExPolytech.2019.8906823.
- [26] A. Feng, D. Chen, C. Li, X. Gu, "Flat-Cladding Fiber Bragg Grating Sensors for Large Strain Amplitude Fatigue Tests", *Sensors*, vol. 10, iss. 8, pp. 7674-7680, Aug. 2010, DOI: 10.3390/s100807674.
- [27] H. Zhang, J. Tersoff, S. Xu, H. Chen, Q. Zhang, K. Zhang, Y. Yang, C.-S. Lee, K.-N. Tu, Ju Li, Y. Lu, "Approaching the ideal elastic strain limit in silicon nanowires", *Science Advances*, vol. 2, no. 8, e1501382 Aug. 2016, DOI: 10.1126/sciadv.1501382.
- [28] A. D. Gomes, M. S. Ferreira, J. Bierlich, J. Kobelke, M. Rothhardt, "Hollow microsphere combined with optical harmonic Vernier effect for strain and temperature discrimination", *Optics & Laser Technology*, vol. 127, p. 106198, Feb. 2020, DOI: 10.1016/j.optlastec.2020.106198.
- [29] P. M. R. Robalinho, A. D. Gomes, O. Frazão, "High Enhancement Strain Sensor based on Vernier Effect using 2-Fiber Loop Mirrors", *IEEE Phot. Techn. Letters*, vol. 32, iss. 18, pp. 1139-1142, Sept. 2020, DOI: 10.1109/LPT.2020.3014695.
- [30] J. Li, M. Zhang, M. Wan, C. Lin, S. Huang, C. Liu, Q. He, X. Qiu, X. Fang, "Ultrasensitive refractive index sensor based on enhanced Vernier effect through cascaded fiber core-offset pairs", *Optics Express*, vol. 28, iss. 3, pp. 4145-4155, Feb. 2020, DOI: 10.1364/OE.384815.
- [31] Shun Liu, Ping Lu, Enci Chen, Wenjun Ni, Deming Liu, Jiangshan Zhang, and Zhenggang Lian. "Vernier effect of fiber interferometer based on cascaded PANDA polarization maintaining fiber." *Chinese Optics Letters*, vol. 17, iss. 8, pp. 080601, Aug 2019.
- [32] H. Le-yi, M. B.-Ning, W. J.-Feng, X. Ben, S. C.-Yu, Z. C.-Liu, "Temperature Characteristics of Cascaded Fabry-Pérot Interferometer Sensors Based on Vernier Effect", *Acta Photonica Sinica*, vol. 48, iss. 9, pp. 906002-0906002, Sep. 2019.
- [33] O. Frazão, J. M. Baptista, J. L. Santos, "Recent Advances in High-Birefringence Fiber Loop Mirror Sensors", *Sensors*, vol. 7, iss. 11, pp. 2970 - 2983, Nov. 2007, DOI: 10.3390/s7112970